APLLIED THERMAL ENGINEERING
VOL.xxx (2014), PP. 1-7
ISSN: 1359-4311
http://www.sciencedirect.com/science/article/pii/S1359431114009259

TITLE:
BUBBLE ACTIVATION FROM A HYDROPHOBIC SPOT AT "NEGATIVE" SURFACE SUPERHEAT IN SUBCOOLED BOILING

APLLIED THERMAL ENGINEERING
VOL.xxx (2014), PP. 1-7
ISSN: 1359-4311
http://www.sciencedirect.com/science/article/pii/S1359431114009259

TITLE:
BUBBLE ACTIVATION FROM A HYDROPHOBIC SPOT AT "NEGATIVE" SURFACE SUPERHEAT IN SUBCOOLED BOILING

PENGESAHAN

1. Judul : Bubble activation from a hydrophobic spot at "negative" surface superheats in subcooled boiling

2. Penulis :

a. Nama : Dr.Eng. Bambang Joko Suroto
b. NIP : 197510282008011009
c. Pangkat/Golongan : Pembina TKI/IIIb
d. Jabatan : Tenaga Pengajar
e. Unit Kerja : Fisika, FMIPA, Universitas Lampung

Telah dimuat di Jurnal "Applied Thermal Engineering".

Bandar Lampung, 21 April 2015

Mengetahui,
Dekan FMIPA, Universitas Lampung

Prof. Suharsi, Ph.D.
NIP. 196905301993121001

Penulis,

Dr.Eng. Bambang Joko Suroto
NIP. 197510282008011009

Ketua Lembaga
Penelitian dan Pengabdian Kepada Masyarakat
Universitas Lampung

Dr.Eng. Admi Syarif
NIP 196701031992031003

Editorial Committee

http://www.journals.elsevier.com/applied-thermal-engineering/

Keterangan sampul :
Cover dari Jurnal ATE (Applied Thermal Engineering)

Guide

Submi

Track

Order

View A

Sponsored Open Access

Sample Issue

Applied Thermal Engineering

Design. Processes. Equipment. Economics

Applied Thermal Engineering publishes original, high-quality research papers and ancillary features, spanning activities ranging from fundamental research to trouble-shooting in existing plant and equipment...

View full aims and scope

Editor-in-Chief: T.S. Zhao
View full editorial board

Journal Metrics

Source Normalized Impact per Paper (SNIP): 2.440

SCImago Journal Rank (SJR): 1.598

Impact Factor: 2.624

5-Year Impact Factor: 2.880

Imprint: ELSEVIER

ISSN: 1359-4311

Related Publications

This journal supports the following content innovations

AudioSlides, Interactive MATLAB Figure Viewer, Nomenclature Viewer

Recent Open Access Articles

Experimental verification of heat transport by acoustic wave
Shinya Hasegawa | Keisuke Kondo | ...

Thermodynamic consistency of the pseudopotential lattice Boltzmann model for simulating liquid–vapor flows
Q. Li | K.H. Luo

A high efficiency 10 kWe microcogenerator based on an Atkinson cycle internal combustion engine
Pietro Capaldi

VIEW ALL

Most Downloaded Articles

1. **Review on thermal energy storage with phase change: materials, heat transfer analysis and applications**
Belén Zalba | José Ma Marín | ...

2. **CFD applications in various heat exchangers design: A review**

Journal Insights

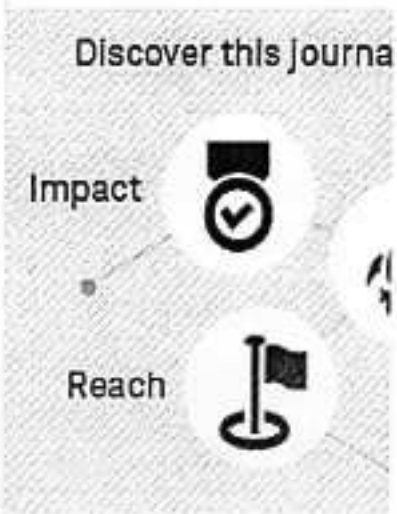

FIND OUT MORE

Most Cited Articles

Pre-combustion, post-combus oxy-combustion in thermal po CO2 capture
Mohamed S. Kanniche | René G

Thermo-economic optimizatio recovery Organic Rankine Cyc
Sylvain Quoilin | Sébastien Deck

An experimental investigation

Muhammad Mahmood Aslam Bhutta | Nasir Hayat | ...

3. Experimental verification of heat transport by acoustic wave
Shinya Hasegawa | Keisuke Kondo | ...

VIEW ALL

Special Issues

6th International Conference on Clean Coal Technologies CCT2013 ORDER NOW
Volume 74 (2015)
Petros A. Pilavachi | Robert Davidson | ...

Special Issue for the 2nd International Workshop on Heat Transfer Advances for Energy Conservation and Pollution Control (IWHT2013) ORDER NOW
Volume 73, Issue 2 (2014)
Qiu-Wang Wang | Bengt Sunden | ...

Special Issue: International Symposium on Innovative Materials for Processes in Energy Systems 2013 (IMPRES2013) ORDER NOW
Volume 72, Issue 2 (2014)
Bidyut Baran Saha | Yasuyuki Takata | ...

VIEW ALL

convective cooling performan microchannel heat sink with A nanofluid
Chingjenq Ho | Lei Wei | ...

VIEW ALL

Recent Articles

Versatile siloxane based adso for fast water adsorption proc thermally driven chillers and h
Harry Kummer | Gerrit Füldner |

Comprehensive performance a optimization of the irreversibl thermodynamic cycle engines maximum power (MP) and ma density (MPD) conditions
Guven Gonca | Bahri Sahin | ...

Mine emissions reduction inst
Piotr Ostrowski | Marek Pronobi

VIEW ALL

Applied Thermal Engineering

Guide for Authors

Submit Your Paper

Track Your Paper

Order Journal

New Articles

Recent Open Access Articles

Open Access Options

Journal Insights

Most Downloaded Articles

Most Cited Articles

Special Issues

Recent Articles

Stay up-to-date

Register your interests and receive email alerts tailored to your needs

Click here to sign up

Follow us

Applied Thermal Engineering Editorial Board

R.Z. Wang

Shanghai Jiao Tong University, Shanghai, China

C. Wu

United States Naval Academy, Annapolis, Maryland, USA

Applied Thermal Engineering xxx (2014) 1–7

Contents lists available at ScienceDirect

Applied Thermal Engineering

journal homepage: www.elsevier.com/locate/apthermeng

Bubble activation from a hydrophobic spot at "negative" surface superheats in subcooled boiling

Bo Shen [a, b, *], Bambang Joko Suroto [b, c], Sana Hirabayashi [b], Masayuki Yamada [b], Sumitomo Hidaka [b], Masamichi Kohno [a, b], Koji Takahashi [a, d], Yasuyuki Takata [a, b]

[a] International Institute for Carbon-Neutral Energy Research (I²CNER), Kyushu University, 744 Motooka, Nishi-ku, Fukuoka 819-0395, Japan
[b] Department of Mechanical Engineering, Kyushu University, 744 Motooka, Nishi-ku, Fukuoka 819-0395, Japan
[c] Department of Physics, Faculty Mathematic and Natural Science, Lampung University, Jl. Prof. Sumantri Brojonegoro No. 1, GedungMeneng, Bandar Lampung 35145, Indonesia
[d] Department of Aeronautics and Astronautics, Kyushu University, 744 Motooka, Nishi-ku, Fukuoka 819-0395, Japan

HIGHLIGHTS

- Bubbles occurred on hydrophobic PTFE spots at nominally negative superheats.
- Bubble departure frequency and diameter were obtained by high-speed imaging.
- Estimate of the bubble content was given based on inner temperature measurements.
- Heat-pipe effect explains the slow bubble growth under the subcooled condition.

ARTICLE INFO

Article history:
Received 20 June 2014
Received in revised form
October 2014
Accepted 14 October 2014
Available online xxx

Keywords:
Bubble dynamics
Mixed wettability
High bubble
Dissolved air
Boiling

ABSTRACT

We present experimental results on the controlled bubble generation from a single PTFE (polytetrafluoroethylene) spot—with diameter varying from 2 mm to 6 mm—deposited on a flat polished copper surface that was submersed in subcooled pure water. The static contact angle of the PTFE coating was measured to be over 120°, which conveniently produced a clear contrast with the copper substrate in terms of wettability that ensured controlled bubble nucleation. By making use of a high-speed camera, statistical details about the bubble formation that include the departure frequency and diameter have been obtained at various surface temperatures. An interesting observation was made of repeated cycles of bubble nucleation and detachment at nominally negative surface superheats (i.e., the wall temperature being below the saturation temperature at the system pressure), which featured particularly long bubble growth time and seemingly no waiting time. The vertical temperature distribution inside the bubble, which was measured by a micro-thermocouple of about 250 μm in diameter, suggests a relatively stable bubble composition of water vapor and dissolved air. A heat-pipe analogy was drawn to describe the internal heat transfer mechanism of bubble growth on a mixed wettability surface under subcooled conditions.

1. Introduction

Due to the large latent heat of evaporation and, perhaps more importantly, strong bubble-induced agitation in the superheated liquid layer [1,2], boiling offers an extremely efficient means of heat transfer and consequently finds a wide range of industrial applications from electronics cooling to refrigeration and cryocoolers to nuclear reactors. The performance of boiling heat transfer depends on two critical parameters: (i) the heat transfer coefficient (HTC), which is defined as the ratio of the imposed heat flux to the corresponding wall superheat $\Delta T_w = T_w - T_{sat}$; and (ii) the critical heat flux (CHF), which demarcates the boundary between the nucleate boiling regime and the less desirable regime of film boiling. The latter stage often entails a dangerous dry-out condition in which the vapor-covered surface is likely to suffer severe physical damages owing to the drastic wall temperature hike.

* Corresponding author. Department of Mechanical Engineering, Kyushu University, 744 Motooka, Nishi-ku, Fukuoka 819-0395, Japan. Tel.: +81 92 802 3905; fax: +81 92 802 3068.
E-mail addresses: shen.bleo604@m.kyushu-u.ac.jp (B. Shen), laks102@yahoo.com (B.J. Suroto), myamada@heat.mech.kyushu-u.ac.jp (M. Yamada), kohno.masamichi.807@m.kyushu-u.ac.jp (M. Kohno), takata@mech.kyushu-u.ac.jp (Y. Takata).

http://dx.doi.org/10.1016/j.applthermaleng.2014.10.054

Please cite this article in press as: B. Shen, et al., Bubble activation from a hydrophobic spot at "negative" surface superheats in subcooled boiling, Applied Thermal Engineering (2014), http://dx.doi.org/10.1016/j.applthermaleng.2014.10.054

Nomenclature

D_d	bubble detachment diameter (m)
f	bubble detachment frequency (s^{-1})
g	acceleration due to gravity ($m\ s^{-2}$)
L	specific latent heat ($kJ\ kg^{-1}$)
ΔT_{sub}	subcooling (°C)
ΔT_{sat}	wall superheat (°C)
T	temperature (°C)
v_{fg}	specific volume change ($m^3\ kg^{-1}$)

Greek symbols

θ	contact angle (°)
λ	thermal conductivity ($W\ m^{-1}\ °C^{-1}$)
σ	surface tension ($N\ m^{-1}$)
ρ	density ($kg\ m^{-3}$)

Subscripts

w	wall
b	bulk
c	copper
l	liquid
p	PTFE
sat	saturation condition
top	near the bubble top
v	vapor

Despite past decades of theoretical, numerical, and experimental efforts [2–5], a comprehensive mechanistic understanding of boiling heat transfer—which accounts for all relevant subprocesses—is still lacking. As a result, most of the recent attempts to enhance boiling efficiency (i.e., HTC and CHF improvements) are either parametrically or empirically based [6,7]. Among the large collection of factors that could potentially affect boiling performance, surface wettability, which is usually measured in terms of the contact angle θ, plays a unique role [8]. On the one hand, hydrophilicity (defined as $\theta < 90°$) can effectively suppress bubble formation and merging, leading to delayed onset of film boiling. Takata et al. [9] demonstrated that TiO_2-coated surfaces, when exposed to UV irradiation, exhibit an unusually high affinity for water (that is, $\theta \approx 0°$). The CHF of pool boiling on such surfaces was found to be about two times that of an uncoated surface. Through nanofluid surface engineering, O'Hanley et al. [10] were able to measure to some extent the individual effect of the wetting property on boiling from other variables such as surface roughness and porosity. The results showed a significantly increased transition temperature for film boiling on porous hydrophilic surfaces, which was attributed to the considerably enlarged capillary force. In nanofluid boiling, surface topology is likely to be modified as a result of nanoparticles deposition, which in turn improves surface wettability and helps explain the exceptionally high CHF [11]. Specifically, the buildup of a porous layer of nanoparticles as a result of microlayer evaporation underneath the growing bubbles can fundamentally alter the surface adhesion tension and wettability, leading to, among other things, significant reduction of contact angle [12]. According to Gerardi et al. [13], the contact angle of the ITO (indium–tin-oxide) heater seemed to drop from about 180° to 6–16° subsequent to being boiled in water-based nanofluids of silica and diamond, respectively. The resulting nanoparticles coatings on the heater surface were found to be responsible for significantly enhanced pool boiling heat transfer due to the pronounced effect of capillary wicking [14,15]. However, the boiling HTC might deteriorate owing to the markedly increased thermal resistance and declining bubble nucleation sites. Forrest et al. [16] reported up to 50% HTC degradation on the superhydrophilic thin-film nanoparticles-deposited surfaces made by the layer-by-layer assembly method. On the other hand, hydrophobicity is known to promote bubble generation, and thus results in greatly improved HTC. By means of electrolytic nickel plating with a suspension of fine PTFE (polytetrafluoroethylene) particles, Takata et al. [17] made a super water-repellent surface (with $\theta > 150°$), on which bubbles appeared at extremely low superheats and quickly coalesced into a vapor film without departing from the surface.

On account of the opposite effects of surface wettability on the boiling CHF and HTC, it requires careful trade-offs between hydrophilicity and hydrophobicity to optimize surface design for boiling applications. Betz et al. [18] were able to create superhydrophobic patterns (made by Teflon fluoropolymer coating) by using photolithography on a silicon wafer that was decorated with random superhydrophilic nanostructures. The resulting so-called *superhiphilic* surface showed remarkable improvements in both the CHF and HTC compared with a plain surface. In our previous study [19], spot coating of PTFE on a hydrophilic TiO_2 surface was found to lead to generally enhanced heat transfer performance. In addition, one interesting observation caught our attention: bubbles actually appearing on the mixed wettability surface at very low—even negative—surface superheats, which was conjectured to be a result of some incondensables inside the bubbles. For subcooled water ($\Delta T_b = T_{sat} - T_b > 0$), for instance, the onset of nucleate boiling (ONB) was found to occur at the surface temperature as low as $T_w = 95.8$ °C, well below the nominal saturation temperature at atmospheric pressure (namely, $T_{sat} = 100.0$ °C). The present work represents our first attempt at understanding the origin of this unexpected phenomenon. By using a high-speed camera, bubble dynamics—including the departure frequency and diameter—on a hybrid surface (polished copper surface coated with a single PTFE spot) was examined. In addition, the temperature distributions within a growing bubble were obtained with the help of a microthermocouple, from which we are able to derive a rough estimate of the vapor/gas bubble content.

2. Experiment apparatus and procedure

A schematic diagram of the pool boiling test facility is shown in Fig. 1. Surrounded by foam insulation, the glass boiling vessel had a volume of about 5 L (450 mm high and 120 mm in diameter). An air heater was used to compensate for heat loss to the surroundings

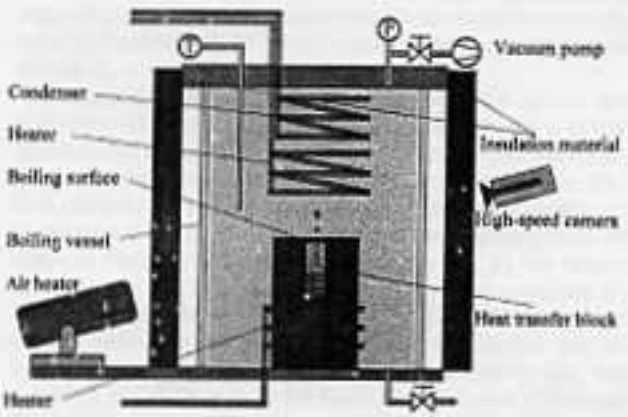

Fig. 1. A schematic representation of the pool boiling experimental setup.

Please cite this article in press as: B. Shen, et al., Bubble activation from a hydrophobic spot at "negative" surface superheats in subcooled boiling, Applied Thermal Engineering (2014), http://dx.doi.org/10.1016/j.applthermaleng.2014.10.054

during the experiment. The bulk water temperature, as measured by a K-type (chromel–alumel junction) thermocouple, was maintained through balancing between an internal water-cooled condenser near the top flange and two electric coil heaters placed above and below the heat transfer block, respectively.

The detailed dimensions of the heat transfer block are shown in Fig. 2(a). On the top of the boiling surface was fitted with an outer ring about 50 mm in diameter and 0.3 mm thick to reduce potential interference of unwanted bubble generation at the border between the copper block and the enclosing stainless plate. At the center of the upward-facing copper surface (polished to a mirror finish by the lapping process with alumina polishing suspensions) was coated with a single PTFE circle of 2 mm, 4 mm, and 6 mm in diameter, respectively [see Fig. 2(b)]. To increase the durability of the surface under boiling conditions, the coated PTFE layer was hardened by thermal treatment at 260 °C. The contact angle of the PTFE spot was measured by the sessile drop technique, the results of which varied between 120 and 127°. The SEM (scanning electron microscope) image of the hybrid surface (Fig. 3) shows a clear contrast with regard to surface topography between the 30-μm thick PTFE layer and the adjacent copper substrate. Due additionally to the relatively low thermal conductivity ($\lambda_P \approx 0.25$ W m^{-1} K^{-1} for PTFE, in comparison with $\lambda_c \approx 400$ W m^{-1} K^{-1} for copper), the rough-textured PTFE-coated subregion provided ample sites for controlled bubble activation.

Heat was applied to the heat transfer block by using two sheathed heaters (SWP1070) with a maximum output power of 700 W. The temperature of the boiling surface was extrapolated, based on a simple one-dimensional (1D) steady-state heat conduction model, from the temperature measurements (with an uncertainty of ±0.2 °C) by using three K-type thermocouples embedded in the heat transfer block along the centerline (at 3 mm, 8 mm, and 13 mm from the top surface, respectively, see Fig. 2(a)). Admittedly, the low thermal conductivity of the PTFE coating could potentially cause local inhomogeneities in the surface heat flux distribution, which leads to some legitimate concerns regarding the validity of the 1D assumption. For this reason, the measurement error of the thermocouples might not represent the true uncertainty in estimating the surface temperature. It should be noted though that due to the extra thermal resistance of the PTFE layer, the 1D model could potentially overestimate the actual surface temperature.

Before the experiment, the boiling vessel was evacuated thoroughly by a vacuum pump so as to remove residual air trapped in the coated surface. The bottom valve was then opened to feed degassed water (as the working fluid) into the vessel through a

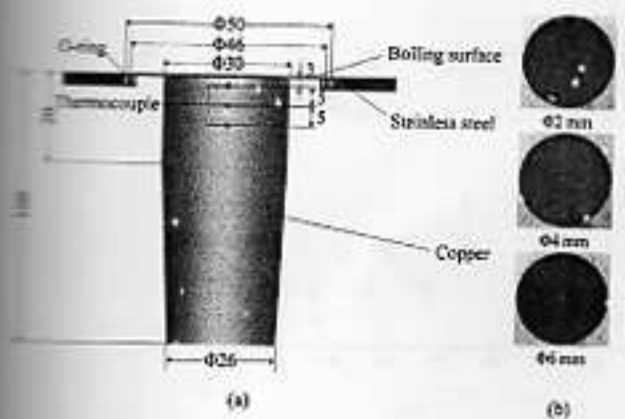

Fig. 2. (a) A schematic representation of the heat transfer block and (b) photos of the PTFE-coated copper surfaces.

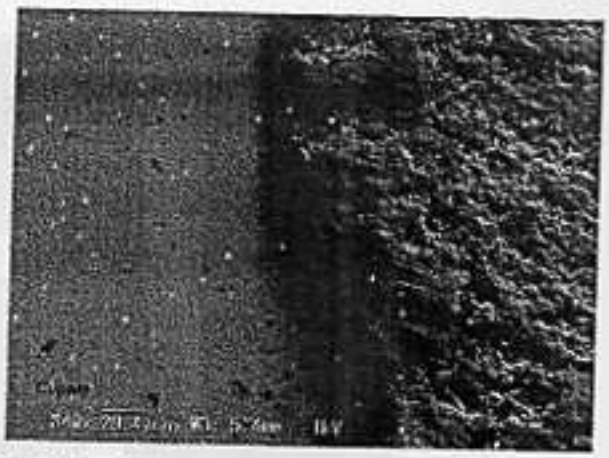

Fig. 3. SEM image of the boundary between the PTFE (with $\theta > 120°$) coating and the copper substrate (with $\theta \approx 70°$).

rubber hose (see Fig. 1). The procedure of degassing through continuous boiling lasted about 30 min. All experiments were performed at atmospheric pressure (with the top of the vessel open to the environment). The bubble behavior (namely, the departure frequency and diameter) was recorded by using a high speed camera (Phantom v.4.3 with a Nikkor 180 mm f/2.8D AF lens) under the subcooled ($\Delta T_b > 0$ °C) and, for comparison, saturation conditions ($\Delta T_b = 0$ °C).

3. Results and discussion

3.1. High-speed visualization of bubble behavior

Fig. 4(a) shows the high-speed images (with a resolution of 640 × 480 obtained at 1900 frames/s) of the bubble departures from the Φ6-mm PTFE spot on the boiling surface at $\Delta T_b = 20$ °C. Consistent with our previous experimental results [19], the first sign of periodic bubble generation was detected at "negative" superheat $\Delta T_w = -2.6$ °C. In contrast, bubbles did not appear until $\Delta T_w = 4.6$ °C under the saturation condition as shown in Fig. 4(b). It has been reported in the literature that bubbles might emerge at very low—even nominally *negative*—wall superheats due largely to the presence of incondensables in the liquid [20,21]. Under subcooled conditions, the water is likely to contain a certain amount of dissolved air in an open system such as the present one, shown in Fig. 1, which could effectively lower the wall temperature threshold for bubble activation as a result of the decreased partial pressure of the vapor phase. Wang et al. [22] found that without any prior degassing processes, bubble embryos started to form on an array of superhydrophobic (PTFE-based nanocomposites) micropatterns at merely $T_w \approx 41.5$ °C in subcooled water.

Notably different from the largely unbounded bubble growth previously observed under subcooled conditions on a uniformly hydrophobic surface [23], where individual bubbles were allowed to spread and merge without eventual detachment from the surface, (partial) bubble departure from the mixed wettability surface is evidenced in Fig. 4(a). On account of the topographical differences at the edge of the PTFE coating (see Fig. 3), the horizontal expansion of the bubble was for the most part confined to the boundary of the hydrophobic subregion. The subsequent vertical growth ultimately led to separation from the surface due to the increased buoyancy force. Immediately following the bubble emission, as can be seen in the figure, the PTFE area still remained blanketed with cone-shaped vapor layer irrespective of the surface temperature—physically defined as local film boiling [19]—as part

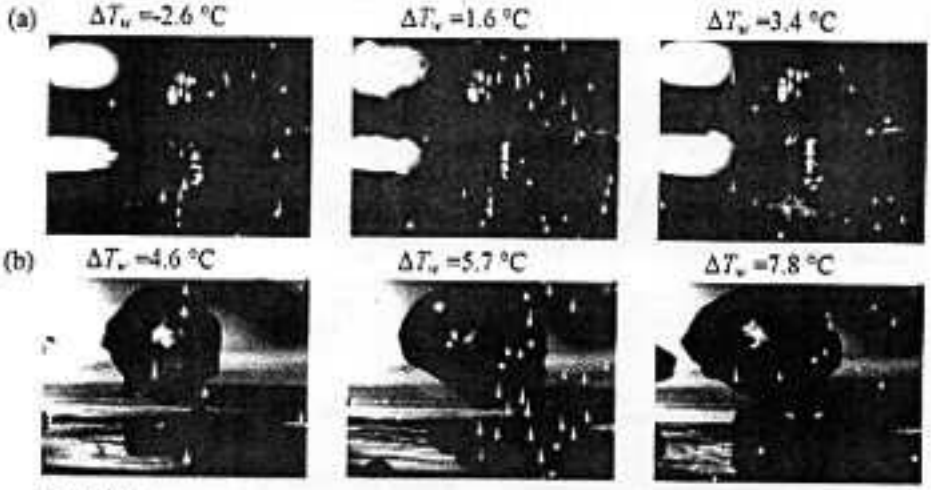

Fig. 4. High-speed still images of the bubble departures from the Φ6-mm PTFE spot on the copper surface under (a) subcooled (ΔT_b = 20 °C) and (b) saturation (ΔT_b = 0 °C) conditions.

of the bubble was apparently left on the surface, which constitutes essentially zero waiting period for bubble generation. It is worth noting that, instead of being completely vapor-capped, the PTFE portion of the surface seemed to be covered with small discrete bubbles under the saturation condition, as shown in Fig. 4(b).

Furthermore, compared with the jagged irregular bubble shapes captured in Fig. 4(b), the bubble interfaces formed in subcooled boiling appeared much smoother (cf. Fig. 4(a)), whose size hardly varied with increasing wall temperature. In the next section, a simple data analysis will be performed to give a quantitative account of the bubble dynamics.

3.2. Statistical analysis of bubble dynamics

Based on the high-speed visualization, statistical details of bubble behavior can be gleaned. Specifically, the bubble departure frequency f_d was determined as the reciprocal of the mean growth time (on account of the zero waiting time) of ten consecutive bubble cycles. In a similar fashion, the departure diameter D_d was defined as the intermediate value between the long and short axes (see Fig. 4) shortly after separation from the surface, also averaged over ten successive bubble departures.

Fig. 5(a) and (b) shows the plots of f_d as a function of the surface temperature T_w for the subcooled (ΔT_b = 20 °C) and saturation (ΔT_b = 0 °C) conditions, respectively. The error bars represent the data scattering. The results clearly indicate that bubble ejection occurred much less frequently in subcooled boiling as f_d for ΔT_b = 20 °C was more than three orders of magnitude lower than that for ΔT_b = 0 °C. Strong condensation from the significantly cooler bulk was largely responsible for the slow bubble buildup, resulting in a particularly long growth period before the final breakoff. Note that during that time, the bubbles, instead of standing perfectly still, appeared to constantly wiggle up and down on the surface.

Independent of the bulk temperature, f_d increased with rising wall temperature for all sizes of the PTFE coating because of the apparently stronger consequent evaporation. Also noteworthy is that, as shown in Fig. 5(a), the f_d versus T_w relation in the negative superheat region ($T_w < T_{sat}$) seemed to follow seamlessly, without any noticeable deviations, the rising trend in the positive territory ($T_w > T_{sat}$), which suggests a consistent bubble growth mechanism at work.

When plotted against the departure diameter D_d, the distributions of f_d exhibit quite different characteristics between the cases of subcooled and saturation boiling. For ΔT_b = 20 °C (see Fig. 6(a)), the bubbles formed from the same PTFE spot at different T_w varied relatively little in size. The increased heat flux resulted mainly in a reduction of the bubble growth time (thus higher f_d). On the other

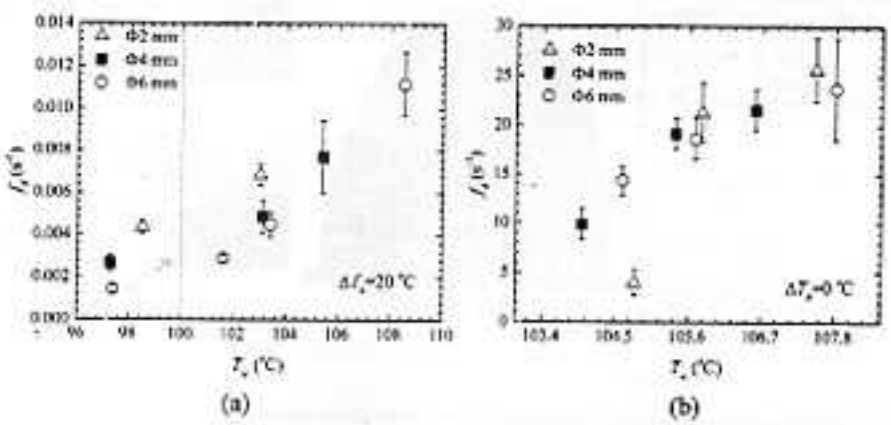

Fig. 5. The relation between the frequency of bubble departure and the surface temperature under (a) the subcooled (ΔT_b = 20 °C) and (b) saturation (ΔT_b = 0 °C) conditions.

Please cite this article in press as: B. Shen, et al., Bubble activation from a hydrophobic spot at "negative" surface superheats in subcooled boiling, Applied Thermal Engineering (2014), http://dx.doi.org/10.1016/j.applthermaleng.2014.10.034

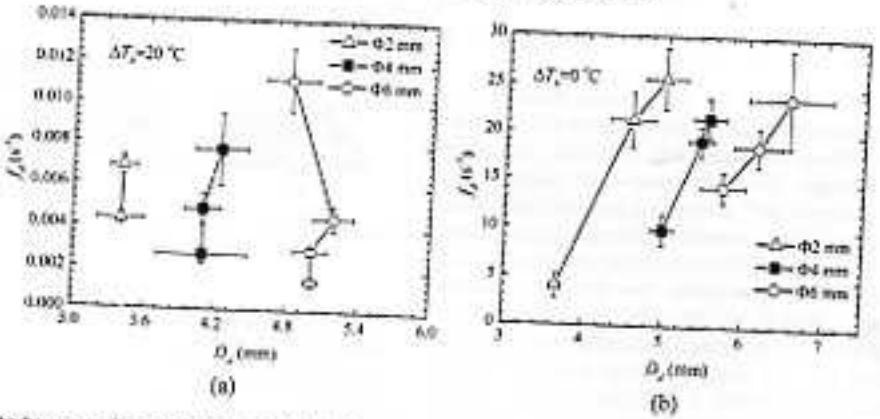

Fig. 6. The relation between the frequency of bubble departure and the bubble diameter under (a) the subcooled ($\Delta T_b = 20$ °C) and (b) saturation ($\Delta T_b = 0$ °C) conditions.

hand, under the saturation condition (see Fig. 6(b)), the bubble expansion did not cease immediately at the moment of detachment as evaporation continued at the bubble interface. Furthermore, due to the thickening of the superheated liquid layer, it seemed that increasingly larger bubbles resulted from the rising surface temperature—at growing frequency, no less. It should be noted that Fuber's correlation [5]

$$f_d D_d = 0.59\left[\frac{\sigma g(\rho_l - \rho_v)}{\rho_l^2}\right]^{1/4} \quad (1)$$

is not applicable here for the bubble growth was limited by the pinning of the (triple-phase) contact line at the edge of the PTFE coating. In Eq. (1) σ is the surface tension, ρ_l the liquid density, ρ_v the vapor density, and g the acceleration due to gravity.

3.2. Effect of dissolved gas

Given that the bubbles remained attached to the hydrophobic subregion in subcooled boiling for an extended period of time (as evidenced in Figs. 5(a) and 6(a)), their inside (temperature) structures can be probed by using a micro-thermocouple with a tip diameter of only 250 μm (see Fig. 7(a)). Note that a similar technique was employed in the detection of an isothermal layer beneath the interface during steady-state water droplet evaporation and condensation [24]. The micro-thermocouple was affixed to a three-axis linear translation positioner that was mounted onto the top flange of the boiling vessel. Encased in a 316 stainless steel sheath with MgO thermal insulation, the chromel–alumel junction was able to provide reliable temperature readings within the vapor phase without causing too much disturbance and distortion to the bubble interface. The measurement error was about ±1.5 °C and the response time was less than 0.015 s.

In Fig. 7(b) are shown the temperature measurements at various vertical positions inside bubbles growing on the Φ6-mm PTFE spot for the case of $\Delta T_b = 20$ °C and on the Φ4-mm PTFE spot for the case of $\Delta T_b = 10$ °C, respectively. Quite interestingly, regardless of the surface superheat, the bubble temperatures in both cases consistently fell well below the nominal saturation temperature. Assuming the bubbles to be composed mainly of a mixture of water vapor and dissolved gas, we describe the heat transfer mechanism based on the heat-pipe effect (Fig. 8): significant condensation in the upper region of the bubble and micro-layer evaporation at the base occurred at reduced saturation temperature thanks to the accumulation of incondensable air. The global thermal balance between the evaporation and condensation processes—bridged mainly by heat conduction (as suggested by the consistent vertical temperature gradients in Fig. 7(b)) —led to the particularly low departure frequencies shown in Figs. 5(a) and 6(a), and the aforementioned continuous oscillations of the bubble interface.

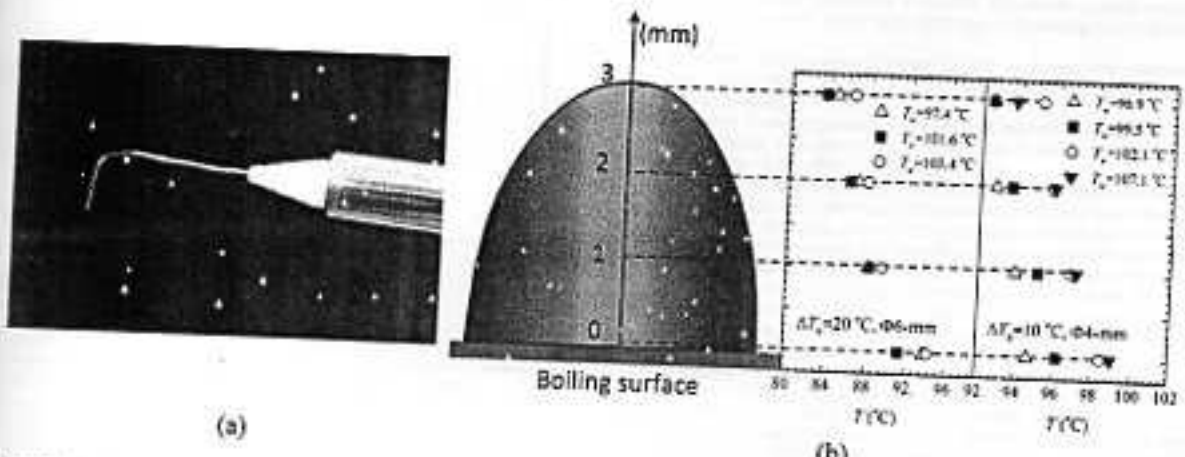

Fig. 7. The inner temperature measurement of a quasi-stationary bubble attached to the PTFE subregion under the subcooled conditions, performed by using a micro-thermocouple as shown in (a). The results in (b) show the temperature distributions were consistently below T_{sat} at atmospheric pressure, suggesting the existence of dissolved air.

Please cite this article in press as: B. Shen, et al., Bubble activation from a hydrophobic spot at "negative" surface superheats in subcooled boiling, Applied Thermal Engineering (2014), http://dx.doi.org/10.1016/j.applthermaleng.2014.10.054

Fig. 8. The internal heat transfer mechanism of an air-rich bubble in subcooled boiling.

The amount of incondensable air can be estimated by the difference between the nominal and actual saturation temperatures. In specific, by virtue of the Clausius–Clapeyron equation, the partial pressure of the dissolved gas in the bubble (Fig. 8) is approximated as,

$$P_g = P_i - P_v = \frac{L}{T_{cap}\Delta v}(T_{sat} - T_{cap}) \quad (2)$$

where T_{cap} denotes the condensation temperature near the apex of the bubble measured by the micro-thermocouple (see Fig. 7(b)). Note the specific latent heat L and the change in specific volume from liquid to vapor Δv are both evaluated using T_{cap} (the local equilibrium temperature). In deriving Eq. (2), the contribution of the surface tension force has been omitted on account of the relatively large bubble size.

Fig. 9 shows the calculated P_g obtained for different PTFE coating diameters under 10 °C and 20 °C subcooling, respectively. It seems that steady levels of dissolved gas were always present in the bubbles, showing no clear sign of declining with varying wall temperature. The relatively stable bubble composition suggests a sustained impact of dissolve air, the amount of which appears to increase with rising bulk temperature as shown in the figure, on subcooled boiling. It should be emphasized that the spatial variation of the concentration of incondensable gas within the bubble is not taken into account herein, which is obviously worth further exploration. As a result, the effect of thermocapillary convection (caused by possibly significant saturation temperature gradients) is excluded from the present simplified model.

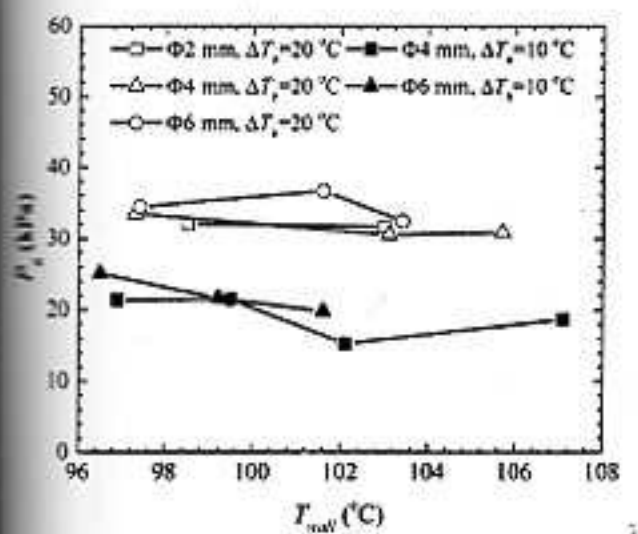

Fig. 9. The estimates of the partial pressure of dissolved gas present in the bubbles formed at different wall temperatures under the subcooled conditions. ΔT_s = 10 and 20 °C.

4. Conclusions

We have carried out an experimental investigation of the controlled bubble growth on the PTFE spot-coated copper surfaces under the subcooled and saturation conditions. Bubble generation at extremely low—even nominally negative—superheats in subcooled boiling was confirmed. The lowering of the incipience for bubble nucleation was attributed to the existence of incondensable gas in the water, whose concentration (partial pressure) within the air/vapor bubbles was determined by making use of the micro-thermocouple. Additionally, the bubble departure frequency and diameter were obtained based on the high-speed image analysis, which exhibited vastly different features between the subcooled and saturation cases. Due to the wettability gap between the PTFE coating and the copper substrate, partial film boiling prevailed on the hydrophobic subregion as no waiting time was observed between successive bubble emissions. Notably the extremely long growth time under the subcooled condition was explained by the heat-pipe effect.

More evidence in regard to the influence of dissolved gas on the bubble formation is currently being sought through experimental efforts to eliminate incondensables from the subcooled water altogether. Some of the preliminary results, which will be presented elsewhere, show that the onset of bubble nucleation could be effectively delayed by creating a "closed" system with thorough degassing. Yet the more puzzling question concerns the initial seeding of air-rich bubble embryos on the hydrophobic surface. Further investigation in this direction could lead to more exciting physics.

Acknowledgements

This work was supported by JSPS KAKENHI Grant Number 24246038. B. Shen gratefully acknowledge financial support by World Premier International Research Center Initiative (WPI), MEXT, and International Institute for Carbon-Neutral Energy Research (WPI-I^{2}CNER), Kyushu University, Japan.

References

[1] H.K. Forster, N. Zuber, Dynamics of vapor bubbles and boiling heat transfer, AIChE J. 1 (1955) 531–535, http://dx.doi.org/10.1002/aic.690010425.
[2] V.K. Dhir, Mechanistic prediction of nucleate boiling heat transfer – achievable or a hopeless task, J. Heat Transfer 128 (2005) 1–12, http://dx.doi.org/10.1115/1.2130366.
[3] B.B. Mikic, W.M. Rohsenow, P. Griffith, On bubble growth rates, Int. J. Heat Mass Transfer 13 (1970) 657–666, http://dx.doi.org/10.1016/0017-9310(70)90040-2.
[4] N. Zuber, The dynamics of vapor bubbles in nonuniform temperature fields, Int. J. Heat Mass Transfer 2 (1961) 83–98, http://dx.doi.org/10.1016/0017-9310(61)90010-3.
[5] N. Zuber, Nucleate boiling. The region of isolated bubbles and the similarity with natural convection, Int. J. Heat Mass Transfer 6 (1963) 53–60, http://dx.doi.org/10.1016/0017-9310(63)90029-2.
[6] I.L. Pioro, W. Rohsenow, S.S. Doerffer, Nucleate pool-boiling heat transfer, I: review of parametric effects of boiling surface, Int. J. Heat Mass Transfer 47 (2004) 5033–5044, http://dx.doi.org/10.1016/j.ijheatmasstransfer.2004.06.019.
[7] I.L. Pioro, W. Rohsenow, S.S. Doerffer, Nucleate pool-boiling heat transfer. II: assessment of prediction methods, Int. J. Heat Mass Transfer 47 (2004) 5045–5057, http://dx.doi.org/10.1016/j.ijheatmasstransfer.2004.06.020.
[8] C.H. Wang, V.K. Dhir, Effect of surface wettability on active nucleation site density during pool boiling of saturated water, J. Heat Transfer 115 (1993) 659–669, http://dx.doi.org/10.1115/1.2910737.
[9] Y. Takata, S. Hidaka, M. Masuda, T. Ito, Pool boiling on a superhydrophilic surface, Int. J. Energy Res. 27 (2003) 111–119, http://dx.doi.org/10.1002/er.861.
[10] H. O'Hanley, C. Coyle, J. Buongiorno, T. McKrell, L.-W. Hu, M. Rubner, R. Cohen, Separate effects of surface roughness, wettability, and porosity on the boiling critical heat flux, Appl. Phys. Lett. 103 (2013) 024102, http://dx.doi.org/10.1063/1.4813450.
[11] S.M. You, J.H. Kim, K.H. Kim, Effect of nanoparticles on critical heat flux of water in pool boiling heat transfer, Appl. Phys. Lett. 83 (2003) 3374–3376, http://dx.doi.org/10.1063/1.1619206.

Please cite this article in press as: B. Shen, et al., Bubble activation from a hydrophobic spot at "negative" surface superheats in subcooled boiling, Applied Thermal Engineering (2014), http://dx.doi.org/10.1016/j.applthermaleng.2014.10.054

[12] S.J. Kim, I.C. Bang, J. Buongiorno, L.-W. Hu, Surface wettability change during pool boiling of nanofluids and its effect on critical heat flux, Int. J. Heat Mass Transfer 50 (2007) 4105–4116, http://dx.doi.org/10.1016/j.ijheatmasstransfer.2007.02.002.

[13] C. Gerardi, J. Buongiorno, L.-W. Hu, T. McKrell, Infrared thermometry study of nanofluids pool boiling phenomena, Nanoscale Res. Lett. 6 (2011) 232, http://dx.doi.org/10.1186/1556-276X-6-232.

[14] R. Chen, M.-C. Lu, V. Srinivasan, Z. Wang, H.H. Cho, A. Majumdar, Nanowires for enhanced boiling heat transfer, Nano Lett. 9 (2009) 548–553, http://dx.doi.org/10.1021/nl8026857.

[15] S.M. Kwark, R. Kumar, G. Moreno, J. Yoo, S.M. You, Pool boiling characteristics of low concentration nanofluids, Int. J. Heat Mass Transfer 53 (2010) 972–981, http://dx.doi.org/10.1016/j.ijheatmasstransfer.2009.11.018.

[16] E. Forrest, E. Williamson, J. Buongiorno, L.-W. Hu, M. Rubner, R. Cohen, Augmentation of nucleate boiling heat transfer and critical heat transfer using nanoparticle thin-film coatings, Int. J. Heat Mass Transfer 53 (2010) 58–67, http://dx.doi.org/10.1016/j.ijheatmasstransfer.2009.10.008.

[17] Y. Takata, S. Hidaka, T. Uraguchi, Boiling feature on a super water-repellent surface, Heat Transfer Eng. 27 (2006) 25–30, http://dx.doi.org/10.1080/01457630600793962.

[18] A.R. Betz, J. Jenkins, C.-J. Kim, D. Attinger, Boiling heat transfer on superhydrophilic, superhydrophobic, and superbiphilic surfaces, Int. J. Heat Mass Transfer 57 (2013) 733–741, http://dx.doi.org/10.1016/j.ijheatmasstransfer.2012.10.080.

[19] B.J. Sureto, M. Tashiro, S. Hirabayashi, S. Hidaka, M. Kohno, Y. Takata, Effects of hydrophobic-spot periphery and subcooling on nucleate pool boiling from a mixed-wettability surface, J. Therm. Sci. Technol. 8 (2013) 294–308, http://dx.doi.org/10.1299/jtst.8.294.

[20] J. Wu, V.K. Dhir, Numerical simulation of dynamics and heat transfer associated with a single bubble in subcooled boiling and in the presence of non-condensables, J. Heat Transfer 133 (2011) 041502, http://dx.doi.org/10.1115/1.4000979.

[21] K.N. Rainey, S.M. You, S. Lee, Effect of pressure, subcooling, and dissolved gas on pool boiling heat transfer from microporous surfaces in FC-72, J. Heat Transfer 125 (2003) 75–83, http://dx.doi.org/10.1115/1.1527890.

[22] X. Wang, S. Zhao, H. Wang, T. Pan, Bubble formation on superhydrophobic-micropatterned copper surfaces, Appl. Therm. Eng. 35 (2012) 112–119, http://dx.doi.org/10.1016/j.applthermaleng.2011.10.012.

[23] H.T. Phan, N. Caney, P. Marty, S. Colasson, J. Gavillet, Surface wettability control by nanocoating: the effects on pool boiling heat transfer and nucleation mechanism, Int. J. Heat Mass Transfer 52 (2009) 5459–5471, http://dx.doi.org/10.1016/j.ijheatmasstransfer.2009.06.032.

[24] C.A. Ward, D. Stanga, Interfacial conditions during evaporation or condensation of water, Phys. Rev. E 64 (2001) 051509, http://dx.doi.org/10.1103/PhysRevE.64.051509.

Please cite this article in press as: B. Shen, et al., Bubble activation from a hydrophobic spot at "negative" surface superheats in subcooled boiling, Applied Thermal Engineering (2014), http://dx.doi.org/10.1016/j.applthermaleng.2014.10.054